日本原子力研究開発機構機関リポジトリ

Japan Atomic Energy Agency Institutional Repository

Thickness-dependent ferromagnetic metal to paramagnetic insulator transition in La$_{0.6}$Sr$_{0.4}$MnO$_3$ thin films studied by x-ray magnetic circular dichroism

G. Shibata,[1,*] K. Yoshimatsu,[1,2] E. Sakai,[2,3] V. R. Singh,[1] V. K. Verma,[1] K. Ishigami,[4] T. Harano,[1] T. Kadono,[1] Y. Takeda,[5] T. Okane,[5] Y. Saitoh,[5] H. Yamagami,[5,6] A. Sawa,[7] H. Kumigashira,[2,3] M. Oshima,[2] T. Koide,[3] and A. Fujimori[1,4,5]

[1]*Department of Physics, University of Tokyo, Bunkyo-ku, Tokyo 113-0033, Japan*

[2]*Department of Applied Chemistry, University of Tokyo, Bunkyo-ku, Tokyo 113-8656, Japan*

[3]*Photon Factory, Institute of Materials Structure Science, High Energy Accelerator Research Organization (KEK), Tsukuba, Ibaraki 305-0801, Japan*

[4]*Department of Complexity Science and Engineering, University of Tokyo, Bunkyo-ku, Tokyo 113-0033, Japan*

[5]*Condensed Matter Science Division, Japan Atomic Energy Agency, Sayo-cho, Sayo-gun, Hyogo 679-5148, Japan*

[6]*Department of Physics, Kyoto Sangyo University, Kyoto 603-8555, Japan*

[7]*National Institute of Advanced Industrial Science and Technology (AIST), Tsukuba, Ibaraki 305-8562, Japan*

Metallic transition-metal oxides undergo a metal-to-insulator transition (MIT) as the film thickness decreases across a critical thickness of several monolayers (MLs), but its driving mechanism remains controversial. We have studied the thickness-dependent MIT of the ferromagnetic metal La$_{0.6}$Sr$_{0.4}$MnO$_3$ by x-ray absorption spectroscopy and x-ray magnetic circular dichroism. As the film thickness was decreased across the critical thickness of the MIT (6–8 ML), a gradual decrease of the ferromagnetic signals and a concomitant increase of paramagnetic signals were observed, while the Mn valence abruptly decreased towards Mn^{3+}. These observations suggest that the ferromagnetic phase gradually and most likely inhomogeneously turns into the paramagnetic phase and both phases abruptly become insulating at the critical thickness.

I. INTRODUCTION

The physical properties of 3d transition-metal oxides (TMOs) are usually controlled by the bandwidth and/or band filling of the 3d bands [1]. Recently, attempts have also been made to control them by the thickness of thin-film samples, namely, by dimensionality [2–10]. In many metallic oxide thin films, including ferromagnetic ones such as La$_{1-x}$Sr$_x$MnO$_3$ (LSMO) [2–5] and SrRuO$_3$ (SRO) [6,7], and paramagnetic ones such as SrVO$_3$ (SVO) [8,9] and LaNiO$_3$ [10], the resistivity increases when the film thickness is decreased, and metal-to-insulator transitions (MITs) occur at a critical thickness of several monolayers (MLs). Evidence for the MITs was found by transport measurements [2,3,6,10] and photoemission spectroscopy (PES) [4,7–9]. According to the PES studies of TMO thin films, the density of states at the Fermi level (E_F) disappears below 4 ML (SRO [7], SVO [8]) to 8 ML (LSMO [4]), resulting in a large insulating gap (of order ∼1 eV) at E_F. In order to explain such MITs, transport theories for conventional metal thin films [11,12], which take into account only surface roughness, predict extremely small critical thicknesses, and one has to invoke strong electron-electron scattering, namely, strong electron correlation. For example, the thickness-dependent MIT of SVO thin films has been considered as a bandwidth-controlled Mott transition caused by the decreased number of nearest-neighbor V atoms [8]. Furthermore, the decrease of the film thickness leads to the lowering of spatial dimension and symmetry, and the increase of interfacial effects, resulting in the changes of the electric and magnetic properties. In LSMO [3,4] as well as in SRO [6], not only metallic conduction but also

ferromagnetism disappears simultaneously. For LSMO thin films, where the number of electrons is not an integer, the simple bandwidth-controlled Mott transition mechanism alone is not sufficient to explain the MIT and one has also to take into account the effect of disorder or local lattice distortion to induce the localization of charge carriers. Therefore, it is important to consider mechanisms such as charge ordering and/or the splitting of the d bands due to the lower structural symmetry at the surface and interface. Such mechanisms are usually accompanied by changes in the magnetic properties. Thus, it is strongly desired to probe both the electronic states and magnetic properties on the microscopic level at the same time as a function of film thickness.

For this purpose, we have investigated the electric and magnetic properties of LSMO ($x = 0.4$) thin films as functions of film thickness using x-ray magnetic circular dichroism (XMCD). XMCD in core-level x-ray absorption spectroscopy (XAS) is a powerful tool to obtain information about the magnetism of specific elements, together with information about the valence states, and is especially suitable for the study of thin films and nanostructures, because it can probe the intrinsic magnetism without contribution from the substrate and other extrinsic effects.

II. EXPERIMENT

LSMO thin films with various thicknesses were fabricated on the TiO$_2$-terminated (001) surface of SrTiO$_3$ (STO) substrates by the laser molecular beam epitaxy (laser-MBE) method. The LSMO thickness ranged from 2 ML to 15 ML. After the deposition, the films were capped with 1 ML of La$_{0.6}$Sr$_{0.4}$TiO$_3$ (LSTO) and then 2 ML of STO [Fig. 1(a)]. The LSTO layer was inserted to keep the local environment
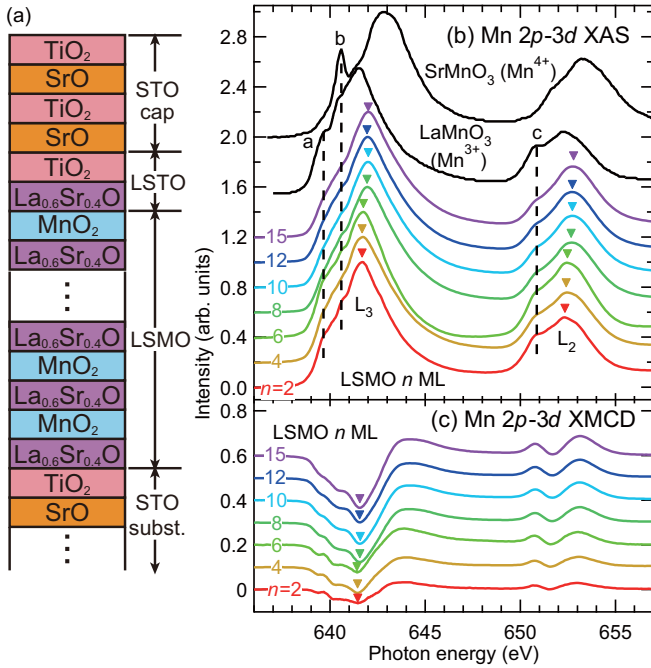
*shibata@wyvern.phys.s.u-tokyo.ac.jp

FIG. 1. (Color online) XAS and XMCD spectra of the La$_{0.6}$Sr$_{0.4}$MnO$_3$ (LSMO) thin films for various thicknesses. (a) Schematic drawing of the thin film samples consisting of LSMO, SrTiO$_3$ (STO), and La$_{0.6}$Sr$_{0.4}$TiO$_3$ (LSTO) layers. (b) Mn $2p$ XAS spectra. (c) Mn $2p$ XMCD spectra. All the spectra were taken at $T = 20$ K with an external magnetic field $\mu_0 H_{\text{ext}} = 3$ T. In panel (b), Mn $2p$ XAS spectra of LaMnO$_3$ (Mn^{3+}) [21] and SrMnO$_3$ (Mn^{4+}) [22] are also shown as references.

FIG. 2. (Color online) Magnetic field dependence of the magnetization (M) of LSMO thin films estimated by XMCD. (a) M plotted against the external field H_{ext}. (b) M plotted against the magnetic field corrected for the demagnetizing field (see text). Inset shows the decomposition of M into the ferromagnetic (M_{ferro}) and paramagnetic (M_{para}) components.

of the topmost MnO$_2$ layer the same as that of the deeper MnO$_2$ layers [4], namely, each MnO$_2$ layer is sandwiched by La$_{0.6}$Sr$_{0.4}$O (LSO) layers. All the fabrication conditions were identical to those of Ref. [4]. The surface morphology of the multilayers was checked by atomic force microscopy, and atomically flat step-and-terrace structures were clearly observed in all the films studied. Four-circle x-ray diffraction measurements confirmed the coherent growth of the films. Prior to measurements, the samples were annealed in 1 atm of O$_2$ at 400 °C for 45 minutes in order to eliminate oxygen vacancies. The XAS and XMCD measurements were performed at polarization-variable undulator beamlines BL-16A of the Photon Factory (PF) and at BL23SU of SPring-8 [13]. The maximum magnetic field was $\mu_0 H_{\text{ext}} = 3$ T at PF and $\mu_0 H_{\text{ext}} = 8$ T at SPring-8. At both beamlines, the magnetic field was applied perpendicular to the film surface. Photons were incident normal to the sample surface and their helicity was reversed to measure XMCD. The measurements were performed at $T = 20$ K. All the spectra were taken in the total electron yield mode. Most of the spectra shown in the figures were taken at PF, while data taken at high magnetic fields ($\mu_0 H_{\text{ext}} > 3$ T) were measured at SPring-8.

III. RESULTS AND DISCUSSION

Figures 1(b) and 1(c) show the XAS and XMCD spectra of all the LSMO samples. The spectral line shapes of XMCD [Fig. 1(c)] are similar to those of bulk LSMO [14].
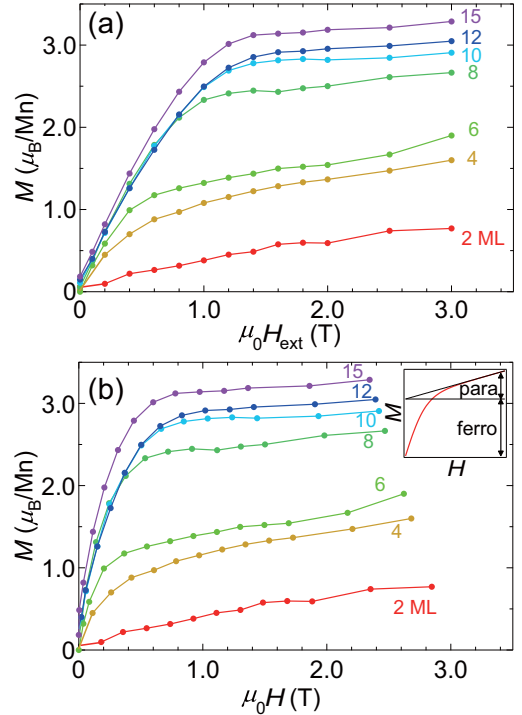
Reflecting the thickness-dependent magnetic properties of LSMO thin films [2–4], the XMCD intensity decreased with decreasing thickness. Using the XMCD sum rules [15,16], we have estimated the spin (M_{spin}) and orbital (M_{orb}) magnetic moments of the Mn ions [17]. The ratio $|M_{\text{orb}}/M_{\text{spin}}|$ was found to be less than $\sim 1/100$ for all the LSMO thicknesses; therefore M_{spin} mainly contributes to the magnetic moment of Mn. Figure 2 shows thus estimated magnetization curves ($M \equiv M_{\text{spin}} + M_{\text{orb}} \sim M_{\text{spin}}$) of the LSMO thin films with various thicknesses. In Fig. 2(a), M's are plotted as functions of applied magnetic field H_{ext}. In Fig. 2(b) the same data are replotted as functions of magnetic field corrected for the demagnetizing field H_{demag} perpendicular to the film as $H = H_{\text{ext}} + H_{\text{demag}} = H_{\text{ext}} - M$. After the demagnetization-field correction, the saturation field is reduced to $\mu_0 H \sim 0.3$–0.8 T, but is still an order of magnitude larger than the saturation field when the external magnetic field is applied parallel to the film and the demagnetizing field is absent ($\mu_0 H \sim 10^{-2}$ T) [18]. Therefore, we conclude that the LSMO thin films have in-plane easy magnetization axes due to magnetocrystalline anisotropy, which probably originates from the tensile strain from the STO substrate [19,20] (note that $a = 0.387$ nm for bulk LSMO while $a = 0.3905$ nm for STO).

Next, we decompose the magnetization curves into two components as shown in the inset of Fig. 2(b): the ferromagnetic component which saturates below $\mu_0 H \sim 1$ T and the paramagnetic component which increases linearly with H up
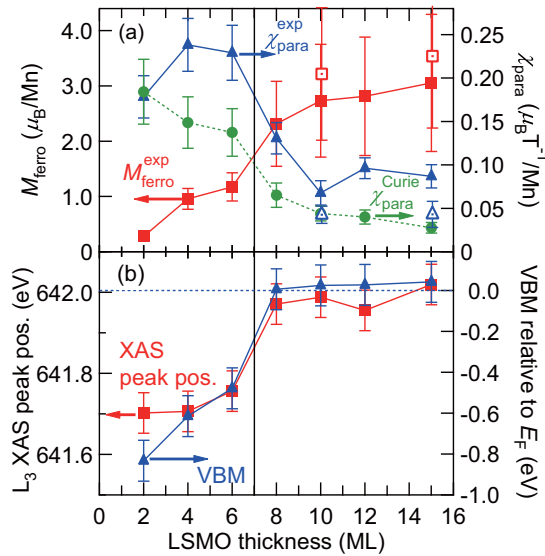
FIG. 3. (Color online) Thickness dependencies of the magnetic and electronic properties of the LSMO thin films. (a) Thickness dependence of the ferromagnetic moment per Mn (M_{ferro}) and the paramagnetic susceptibility (χ_{para}) per Mn of the LSMO thin films, estimated from the magnetization curves in Fig. 2. The paramagnetic susceptibility simulated using the Curie law (χ_{para}^{Curie}) is shown by a dashed curve, indicating an enhancement of the paramagnetic signals. The M_{ferro} and χ_{para} estimated from the magnetization measurements up to $\mu_0 H_{ext} \leqslant 8$ T are shown by open symbols. (b) Peak position of the Mn L_3 edge estimated from the XAS spectra and the valence band maximum (VBM) position relative to the Fermi level (E_F) measured by PES [4].

to the highest magnetic fields [23]. Thus the intercept of the magnetization curve gives the ferromagnetic moment M_{ferro} and the slope of the magnetization curve gives paramagnetic susceptibility χ_{para} of the Mn ions. We confirmed the linear increase of M as a function of H up to higher magnetic fields (3 T $< \mu_0 H_{ext} \leqslant 8$ T) for several samples (not shown), which justifies the separation of the magnetization curves into the ferromagnetic and paramagnetic components. In Fig. 3(a), the M_{ferro} and χ_{para} values thus obtained are plotted as functions of film thickness. With decreasing film thickness, M_{ferro} decreases and χ_{para} increases, indicating a gradual transition from the ferromagnetic state to the paramagnetic state. The measured χ_{para} is, however, somewhat larger than the one predicted by the Curie law of the Mn^{3+}-Mn^{4+} mixed valence state in the entire thickness range [24]. This indicates that the system exhibits a ferromagnetic-to-paramagnetic phase separation and that even in the paramagnetic state there are ferromagnetic correlations between the Mn local moments.

We note that while the thickness-dependent MIT occurs rather abruptly according to PES [4], Fig. 3(a) shows a *gradual* decrease and increase of the ferromagnetic and paramagnetic components, respectively, with decreasing film thickness. Indeed, the thickness dependence of the valence-band maximum (VBM) measured by PES [4], as shown in Fig. 3(b), indicates an abrupt opening of the energy gap below the critical thickness. This means that the paramagnetic component already exists slightly above the critical thickness of the MIT and the ferromagnetic component persists below

it as an ferromagnetic insulating (FM-I) phase. Therefore, the present results suggest that a paramagnetic metallic (PM-M) or paramagnetic insulating (PM-I) phase starts to appear in the ferromagnetic metallic (FM-M) phase from slightly above the critical thickness, and that the FM-I and the PM-I phases coexist below the critical thickness of MIT.

In order to obtain the information about changes in the electronic structure across the MIT, we examine the thickness dependence of the line shapes and the energy positions of the XAS and XMCD spectra. Comparing the experimental XAS spectra with those of LaMnO$_3$ (Mn^{3+}) [21] and SrMnO$_3$ (Mn^{4+}) [22] [Fig. 1(b)], the intensities of structures a and c, which originate from Mn^{3+}, become stronger when the LSMO thickness is reduced. In addition, as shown in Figs. 1(b) and 3(b), the peak positions of the Mn L_3 and L_2 edges are abruptly shifted to lower energies by ~0.2 eV between 8 ML and 6 ML, where the thickness-dependent MIT occurs [4]. Similar peak shifts are also observed in the XMCD spectra, as shown in Fig. 1(c). In the reference XAS spectra in Fig. 1(b), both the L_3 and L_2 edges are located at lower photon energies for Mn^{3+} than for Mn^{4+}. From these spectral changes, we conclude that the effective hole concentration decreases as the LSMO thickness decreases, and that it suddenly drops at the critical thickness of MIT. Considering that bulk LSMO enters the FM-I phase in the low hole concentration region $0.09 \lesssim x \lesssim 0.16$ [25], the observed valence shift towards Mn^{3+} in the thin films is certainly related with the FM-M to FM-I transition with decreasing thickness.

The observed valence change towards Mn^{3+} with decreasing film thickness may be partly explained by the presence of the LSTO layer in the cap. As mentioned in Sec. II a 1-ML-thick LSTO layer is inserted between the LSMO film and the STO cap layer in our samples [Fig. 1(a)]. The (LSO)$^{0.6+}$ layer in LSTO acts as an electron donor. Because the work function of STO is smaller than that of LSMO, the electrons supplied by the LSO layer are doped into the LSMO side rather than the STO side [26]. Thus the average Mn valence is shifted towards the 3+ side from the nominal valence 3.4+. This effect is more significant in the thinner films because the number of the doped electrons per monolayer is larger. However, the amount of electron charges is not enough to explain the observed valence change. There is also a possibility that some oxygen vacancies may exist in the LSMO films and/or STO substrates, which leads to additional electron doping. We note that such a valence change towards Mn^{3+} with decreasing film thickness has also been reported in previous studies [27,28].

The coincidence of the MIT and the abrupt valence change at 6–8 ML implies some connection between the MIT and the valence change. One possible scenario is that the MIT induces changes in the charge distribution in the LSMO film, leading to the apparent decrease of the hole concentration over the entire LSMO film. When the film is thick and metallic, the free electric charges (holes) will be distributed at the top and bottom interfaces of LSMO, so that there is no potential gradient inside the film. When the film becomes thinner and insulating, the holes are distributed over the entire LSMO layer. If the holes at the bottom interface are distributed in a more extended region, it may cause the abrupt Mn valence change observed by XMCD (the probing depth of which is 3–5 nm [29] or 8–12 ML). In order to clarify the relationship

between the observed valence change and the MIT, further experiments would be required, especially on the depth profiles of the electronic states and magnetism in the LSMO thin films.

IV. SUMMARY

We have performed XAS and XMCD studies of LSMO thin films with varying thickness in order to investigate the origin of the thickness-dependent MIT and the concomitant loss of ferromagnetism. With decreasing film thickness, a gradual decrease of the ferromagnetic component and an increase of the paramagnetic component were observed. The experimental paramagnetic susceptibility was larger than the Curie law, indicating that spin correlations between Mn atoms are ferromagnetic. The Mn valence was found to approach Mn^{3+} below the critical thickness of the MIT. The ferromagnetic-to-paramagnetic transition occurred gradually as a function of thickness, whereas the MIT and the valence change towards Mn^{3+} took place abruptly. These results can be understood within the picture of mixed phases: the films above the critical thickness as a mixture of the FM-M and PM-I or PM-M phases while the films below the critical thickness as a mixture of the FM-I and PM-I phases. The mechanism of the valence change has to be investigated as a future theoretical problem.

[1] M. Imada, A. Fujimori, and Y. Tokura, Rev. Mod. Phys. **70**, 1039 (1998).

[2] X. Hong, A. Posadas, and C. H. Ahn, Appl. Phys. Lett. **86**, 142501 (2005).

[3] M. Huijben, L. W. Martin, Y.-H. Chu, M. B. Holcomb, P. Yu, G. Rijnders, D. H. A. Blank, and R. Ramesh, Phys. Rev. B **78**, 094413 (2008).

[4] K. Yoshimatsu, K. Horiba, H. Kumigashira, E. Ikenaga, and M. Oshima, Appl. Phys. Lett. **94**, 071901 (2009).

[5] H. Boschker, J. Kautz, E. P. Houwman, W. Siemons, D. H. A. Blank, M. Huijben, G. Koster, A. Vailionis, and G. Rijnders, Phys. Rev. Lett. **109**, 157207 (2012).

[6] J. Xia, W. Siemons, G. Koster, M. R. Beasley, and A. Kapitulnik, Phys. Rev. B **79**, 140407 (2009).

[7] D. Toyota, I. Ohkubo, H. Kumigashira, M. Oshima, T. Ohnishi, M. Lippmaa, M. Takizawa, A. Fujimori, K. Ono, M. Kawasaki, and H. Koinuma, Appl. Phys. Lett. **87**, 162508 (2005).

[8] K. Yoshimatsu, T. Okabe, H. Kumigashira, S. Okamoto, S. Aizaki, A. Fujimori, and M. Oshima, Phys. Rev. Lett. **104**, 147601 (2010).

[9] K. Yoshimatsu, K. Horiba, H. Kumigashira, T. Yoshida, A. Fujimori, and M. Oshima, Science **333**, 319 (2011).

[10] R. Scherwitzl, S. Gariglio, M. Gabay, P. Zubko, M. Gibert, and J.-M. Triscone, Phys. Rev. Lett. **106**, 246403 (2011).

[11] K. Fuchs, Proc. Cambridge Philos. Soc. **34**, 100 (1938).

[12] E. H. Sondheimer, Phys. Rev. **80**, 401 (1950).

[13] Y. Saitoh, Y. Fukuda, Y. Takeda, H. Yamagami, S. Takahashi, Y. Asano, T. Hara, K. Shirasawa, M. Takeuchi, T. Tanaka, and H. Kitamura, J. Synchrotron Radiat. **19**, 388 (2012).

[14] T. Koide, H. Miyauchi, J. Okamoto, T. Shidara, T. Sekine, T. Saitoh, A. Fujimori, H. Fukutani, M. Takano, and Y. Takeda, Phys. Rev. Lett. **87**, 246404 (2001).

[15] B. T. Thole, P. Carra, F. Sette, and G. van der Laan, Phys. Rev. Lett. **68**, 1943 (1992).

[16] P. Carra, B. T. Thole, M. Altarelli, and X. Wang, Phys. Rev. Lett. **70**, 694 (1993).

[17] Since the spin sum rule tends to underestimate the magnetic moment when spin-orbit splitting of the transition-metal $2p$ core levels is not large enough compared to the $2p$-$3d$ exchange splitting interaction, we have divided M_{spin} by a "correction factor" 0.587 given in Y. Teramura, A. Tanaka, and T. Jo, J. Phys. Soc. Jpn. **65**, 1053 (1996).

[18] Y. Ishii, H. Yamada, H. Sato, H. Akoh, M. Kawasaki, and Y. Tokura, Appl. Phys. Lett. **87**, 022509 (2005).

[19] Y. Konishi, Z. Fang, M. Izumi, T. Manako, M. Kasai, H. Kuwahara, M. Kawasaki, K. Terakura, and Y. Tokura, J. Phys. Soc. Jpn. **68**, 3790 (1999).

[20] D. Pesquera, G. Herranz, A. Barla, E. Pellegrin, F. Bondino, E. Magnano, F. Sanchez, and J. Fontcuberta, Nat. Commun. **3**, 1189 (2012).

[21] T. Burnus, Z. Hu, H. H. Hsieh, V. L. J. Joly, P. A. Joy, M. W. Haverkort, H. Wu, A. Tanaka, H.-J. Lin, C. T. Chen, and L. H. Tjeng, Phys. Rev. B **77**, 125124 (2008).

[22] R. K. Sahu, Z. Hu, M. L. Rao, S. S. Manoharan, T. Schmidt, B. Richter, M. Knupfer, M. Golden, J. Fink, and C. M. Schneider, Phys. Rev. B **66**, 144415 (2002).

[23] Examples of such a decomposition of the magnetization curves can be seen in references, e.g., Y. Takeda, M. Kobayashi, T. Okane, T. Ohkochi, J. Okamoto, Y. Saitoh, K. Kobayashi, H. Yamagami, A. Fujimori, A. Tanaka, J. Okabayashi, M. Oshima, S. Ohya, P. N. Hai, and M. Tanaka, Phys. Rev. Lett. **100**, 247202 (2008).

[24] We have compared the magnitude of χ_{para} with that of noninteracting Mn^{3+}/Mn^{4+} local moments calculated for the Curie paramagnetic state, namely,

$$\chi_{para}^{Curie} = \frac{S(S+1)g^2\mu_B}{3k_B T}\left(1 - \frac{M_{ferro}}{M_0}\right),$$

where $g \simeq 2.0$ is the g factor, $M_0 = 3.6\ \mu_B/Mn$ is the saturation magnetization of LSMO, and $1 - M_{ferro}/M_0$ is the number ratio of the paramagnetic Mn atoms.

[25] A. Urushibara, Y. Moritomo, T. Arima, A. Asamitsu, G. Kido, and Y. Tokura, Phys. Rev. B **51**, 14103 (1995).

[26] H. Kumigashira, A. Chikamatsu, R. Hashimoto, M. Oshima, T. Ohnishi, M. Lippmaa, H. Wadati, A. Fujimori, K. Ono,

M. Kawasaki, and H. Koinuma, Appl. Phys. Lett. **88**, 192504 (2006).

[27] J.-S. Lee, D. A. Arena, P. Yu, C. S. Nelson, R. Fan, C. J. Kinane, S. Langridge, M. D. Rossell, R. Ramesh, and C.-C. Kao, Phys. Rev. Lett. **105**, 257204 (2010).

[28] F. Sandiumenge, J. Santiso, L. Balcells, Z. Konstantinovic, J. Roqueta, A. Pomar, J. P. Espinós, and B. Martínez, Phys. Rev. Lett. **110**, 107206 (2013).

[29] R. Nakajima, J. Stöhr, and Y. U. Idzerda, Phys. Rev. B **59**, 6421 (1999).